Check for updates

Received: 18 November 2022 | Revised: 13 December 2022 | Accepted: 5 January 2023

DOI: 10.1002/aoc.7017

RESEARCH ARTICLE

Applied Organometallic Chemistry WILEY

Magnetic Cu/Co nanoparticles supported on nitrogen-doped porous carbon derived from Cu/Co@aZIF: Investigation of catalytic activity and structural properties

Nesrin Buğday[1] | **Sedat Yaşar**[1] | **Serdar Altin**[2] | **Ozgur Duygulu**[3] | **Yunus Önal**[4]

[1]Department of Chemistry, İnönü University, Malatya, 44280, Turkey

[2]Department of Physics, İnönü University, Malatya, 44280, Turkey

[3]Materials Technologies, TÜBİTAK Marmara Research Center, TÜBİTAK Gebze Campus, Gebze, Kocaeli, 41470, Turkey

[4]Department of Chemistry Engineering, İnönü University, Malatya, 44280, Turkey

Correspondence
Sedat Yaşar, İnönü University, Department of Chemistry, 44280, Malatya, Türkiye.
Email: sedat.yasar@inonu.edu.tr

Funding information
The authors declare that they have no known competing financial support for this work.

By calcining copper-doped amorphous zeolitic imidazolate framework (Cu/Co@aZIF), a novel magnetic nanoporous carbon composite (Cu/Co@NPC) material was produced, characterized by different spectroscopic techniques, and used for the first time as an efficient catalyst for the azide-alkyne cycloaddition (AAC) reaction and the reduction reaction of nitrophenol (RRN) under air in water. With this catalyst, the AAC and RRN reactions were conducted in aqueous solutions, and good to excellent yields of related products were synthesized in a short reaction time. The potential of the magnetic Cu/Co@NPC nanocatalyst for targeting RRN and AAC reactions was uncovered by studying specific substrates for RRN and AAC reactions. The Cu/Co@NPC magnetic nanocatalyst is recyclable at least five times, with just a drop of 6% and 22% in catalytic efficiency in RRN and AAC, respectively.

KEYWORDS
AAC reaction, copper, MOF, nitrophenol, porous carbon

1 | INTRODUCTION

Metal–organic frameworks (MOFs) are a family of materials consisting of metal ions or clusters linked to organic linkers to produce one-, two-, or three-dimensional networks.[1] MOFs have garnered a great deal of interest in the field of catalysis because of their inherent physical and chemical properties.[2–4] MOFs' superior structure allows for faster ion and electron transport as well as increased substrate permeability and more catalytic active sites, all of which are essential for catalytic activity. Facile fabrication, a large specific surface area, high porosity, and easy modification using bridging metal atoms and nitrogen-containing ligands are just a few of the ways in which MOFs outperform traditional porous carbons and inorganic zeolites. On account of these merits, MOFs are a promising catalyst material or support material in many organic transformations.[5–9]

Copper compounds are found in a wide range of catalytic systems because of their diverse redox properties, low cost, biological significance, and extensive chemistry.[10,11] Because the Meldal and Sharpless groups discovered the copper(I)-catalyzed Huisgen 1,3-dipolar cycloaddition of organic azides and alkynes (CuAAC), a number of methods have sprung up around this reaction.[12,13] This reaction has garnered a great deal of interest and has potential applications in materials science, organic synthesis, and medicinal chemistry.[14–16] Heterogeneous catalysis is a dynamic field and has utilized a variety of support material derivatives.[17–20] For the azide-alkyne click cycloaddition process, heterogeneous

 © 2023 John Wiley & Sons Ltd.

10990739, 2023, 3, Downloaded from https://onlinelibrary.wiley.com/doi/10.1002/aoc.7017 by T C Inonu University, Wiley Online Library on [19/02/2023]. See the Terms and Conditions (https://onlinelibrary.wiley.com/terms-and-conditions) on Wiley Online Library for rules of use; OA articles are governed by the applicable Creative Commons License

catalysts made of bare orN-heterocyclic carbene (NHC)-modified silica, zeolites, carbon-based materials, polymeric materials, MOFs, metal nanoparticles (MNPs), and metal-oxide nanoparticles (MONPs) have been examined.[12,21] Among the MOFs used in heterogeneous catalysis, the copper MOF (Cu-MOF) has emerged as a potent and effective catalyst in numerous transformations because of copper's availability, low toxicity, and reasonable cost.[2] However, magnetically separable Cu-doped Zeolitic imidazolate framework (ZIF)-based carbon compounds do not have widespread application.[22] Therefore, it appears difficult to tune the synthesis of copper catalysts to achieve high catalytic efficiency, exceptional selectivity, high stability, and acceptable recyclability.[21]

4-Nitrophenol (4-NP) is a nitro compound that is widespread in the environment and resistant to natural degradation. It is often used as an intermediary in the production of colors, insecticides, and pharmaceuticals.[23–25] It has a high bioavailability in water because it is polar and easily soluble in water.[26] At the same time, because of the rapid improvement of the industry and agriculture, a larger amount of 4-NP-containing wastewater will be released into the environment. Even worse, it has been demonstrated to have harmful effects on the internal organs, brain systems, and blood of humans and animals.[27] Therefore, rapid 4-NP separation from the living environment is of primary importance.[28] For this purpose, adsorption,[29] oxidation process,[30] photocatalytic degradation,[31] and catalytic degradation[32] methods have been developed to eliminate this organic contamination. Catalytic reductive degradation is one such process and is used to convert 4-NP to 4-aminophenol (4-AP), which is another type of commonly utilized industrial substance.[33]

Many research and development efforts have focused on creating low-priced catalysts to compete with more expensive catalysts based on noble metals. Particular interest has been focused on copper nanoparticles (Cu-NPs) among the non-noble metals because of their unique electronic orbital structure, inexpensive cost, and earth richness.[34] When utilized in place of non-noble metals, Cu-NPs catalyze the hydrogenation of nitroaromatic compounds at ambient temperature with a very high conversion rate.[35] However, the high surface energy of Cu-NPs makes it suitable to agglomerate during the reaction, which leads to reduced catalytic activity, stability, and reusability.[36] To prevent these drawbacks, especially agglomeration of MNPs, the common way is to reduce the surface energy of the MNPs by capsulation with a carbon network derived from MOFs.[2]

In this work, we reported synthesis and characterization of a magnetic Cu/Co@Nitrogen-doped porous carbon (NPC) that can be used as an efficient and regioselective heterogeneous catalyst for the azide-alkyne cycloaddition (AAC) reaction to produce substituted triazoles and reduction of nitrophenols to aminophenols in water.

2 | EXPERIMENTAL

2.1 | Chemicals

$Co(NO_3)_2{\cdot}6H_2O$, $Cu(NO_3)_2{\cdot}3H_2O$, benzimidazole (BIM), 4-NP, 3-nitrophenol, 2,4-dinitrophenol, NH_4OH, and other chemicals were purchased from Sigma Aldrich and Alfa Aesar and used as obtained.

2.2 | Measurements and characterization

The detail of characterization is available in the Supporting Information section.

2.3 | Synthesis

2.3.1 | Synthesis of Cu/Co-NPs and Cu/Co@NPC catalysts

Cu/Co-NPs and Cu/Co@NPC were synthesized according to relevant literature with modifications (Figure 1).[2,36] To compare the catalytic activity of the Cu/Co@NPC catalyst with that of the Co@NPC catalyst, the Co@NPC catalyst was produced in accordance with the literature.[8,37] A detailed synthesis procedure is presented in the Supporting Information.

2.3.2 | Synthesis of substituted-1,2,3-triazoles via the CuAAC reaction

A detailed synthesis procedure is presented in Figure 2 and in the Supporting Information.

2.3.3 | Catalytic reduction of nitrophenol derivatives

A detailed synthesis procedure is presented in the Supporting Information.

10990739, 2023, 3, Downloaded from https://onlinelibrary.wiley.com/doi/10.1002/aoc.7017 by T C Inonu University, Wiley Online Library on [19/02/2023]. See the Terms and Conditions (https://onlinelibrary.wiley.com/terms-and-conditions) on Wiley Online Library for rules of use; OA articles are governed by the applicable Creative Commons License

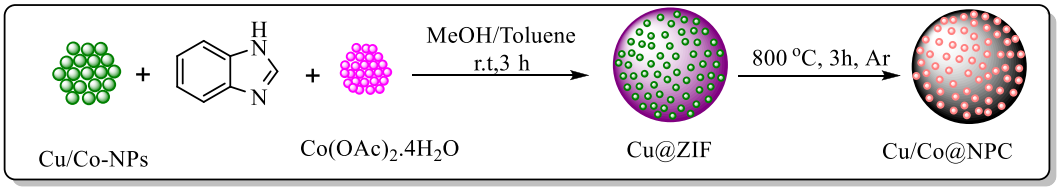


FIGURE 1 The synthesis pathway for the magnetic Cu/Co@ Nitrogen-doped porous carbon(NPC) nanocatalyst

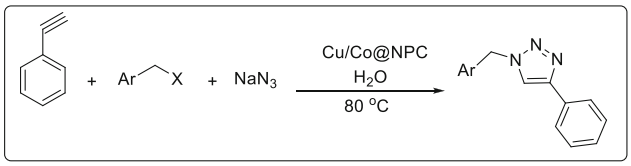


FIGURE 2 General reaction for the synthesis of triazoles catalyzed by Cu/Co@Nitrogen-doped porous carbon NPC

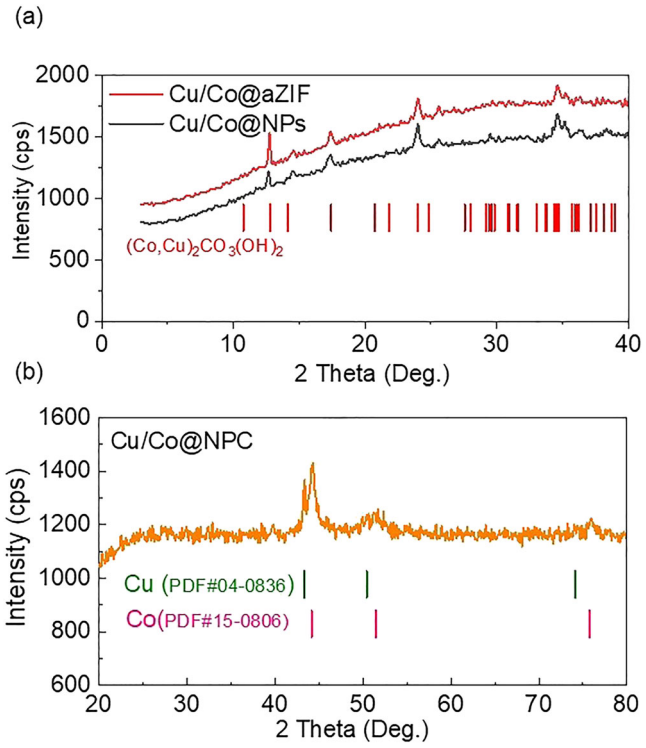


FIGURE 3 X-ray powder diffraction (XRD) pattern of Cu/Co-NPs and Cu/Co@a Zeolitic imidazolate framework (ZIF) (a) and Cu/Co@NPC (b)

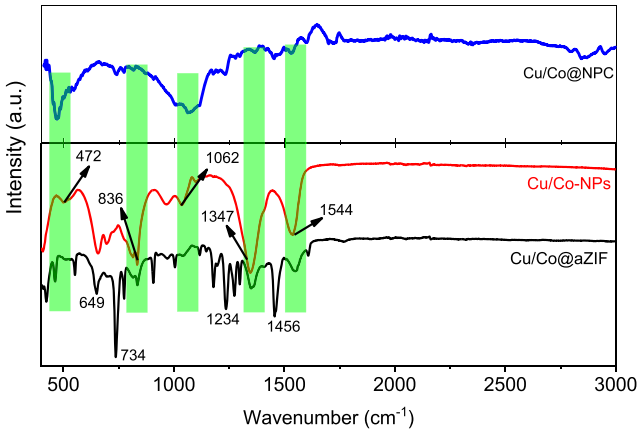


FIGURE 4 Fourier transform infrared (FT-IR) spectra of Cu/Co@aZeolitic imidazolate framework (ZIF), Cu/Co-NPs, and Cu/Co@Nitrogen-doped porous carbon (NPC)

3 | RESULTS AND DISCUSSION

3.1 | Structural properties

Structural characterization of all synthesized materials was started with X-ray powder diffraction (XRD) analysis (Figure 3a,b). As can be seen in Figure 3a, the XRD pattern of Cu/Co-NPs is consistent with the $(Cu,Co)_2CO_3(OH)_2$ phase. In the XRD analysis of Cu/Co@aZIF, a crystalline phase of $(Cu,Co)_2CO_3(OH)_2$ and an amorphous ZIF (aZIF) were detected. The transmission electron microscopy (TEM) analysis of Cu/Co@aZIF has confirmed this discovery, too. As shown in the section on TEM analysis (Figure S2a), the Cu/Co@aZIF phase is composed of crystalline $(Cu,Co)_2CO_3(OH)_2$ and amorphous carbon-based phases. When the Cu/Co@aZIF was carbonized under an Ar atmosphere at a high temperature, elemental Cu (cubic Fm3m) and Co (cubic Fm3m) phases were found together with an amorphous-type carbon structure at about 20° in the XRD pattern (Figure 3b).

The Fourier transform infrared (FT-IR) spectra of Cu/Co@aZIF, Cu/Co-NPs, and Cu/Co@NPC are presented in Figure 4. The C–C stretching vibration of the BIM ring is assigned a peak at 1544 cm^{-1}. The entire ring stretching is related to the intense and convoluted bands around 1456–1347 cm^{-1}. Peaks in the spectrum range 1234, 1062, and 836 cm^{-1} are related to in-plane bending of the BIM ring, whereas bands at 734 and 649 cm^{-1} are associated with out-of-plane bending. The peaks at 472 cm^{-1} were due to the Cu-N/Co-N stretching vibration of the Cu/Co@aZIF, Cu/Co-NPs, and Cu/Co@NPC. This suggests the successful coordination of Cu and Co with BIM.[38,39]

10990739, 2023, 3, Downloaded from https://onlinelibrary.wiley.com/doi/10.1002/aoc.7017 by T C Inonu University, Wiley Online Library on [19/02/2023]. See the Terms and Conditions (https://onlinelibrary.wiley.com/terms-and-conditions) on Wiley Online Library for rules of use; OA articles are governed by the applicable Creative Commons License

The structural characterization of Cu/Co@aZIF and Cu/Co@NPC was continued with TEM analysis. Details concerning the microstructure of the materials can be seen in TEM pictures of Cu/Co@aZIF and Cu/Co@NPC (Figure S2). Low-magnification TEM images (Figure 5a) show the homogenous distribution of particles with spherical morphology. Also, an agglomeration of nanoparticles was observed in dark regions. Figure 5b,c clearly shows the composite structure of the main carbon matrix and the Co/Cu particles. The spherical Co/Cu nanoparticles are crystalline with a size of ∼5–10 nm. Lattice distances measured from the TEM image in Figure 5e and Fast Fournier Transform (FFT) diffractogram (Figure 5f) match the d-spacings of the Co/Cu phase. The d-space, reflection plane, and 2θ values of Co (Fm3m) and Cu (Fe3m) species obtained from XRD and Selected area (electron) diffraction(SAED) measurements are presented in Table 1, showing that the SAED data support the XRD calculation. According to Energy-dispersive X-ray spectroscopy(EDS) analysis, the samples have a homogeneous C, Co, and Cu distribution. SEM-EDS elemental mappings also illustrate that N, Co, and Cu nanoparticles show a uniform distribution throughout the Cu/Co@NPC catalyst (Figure S1d).

The TEM image of the used catalyst (Figure S2c) shows similar structural properties to fresh catalysts. Although some deformation in the crystalline phase was observed, it can be said that the structural properties of the catalyst are almost unchanged after five catalytic processes.

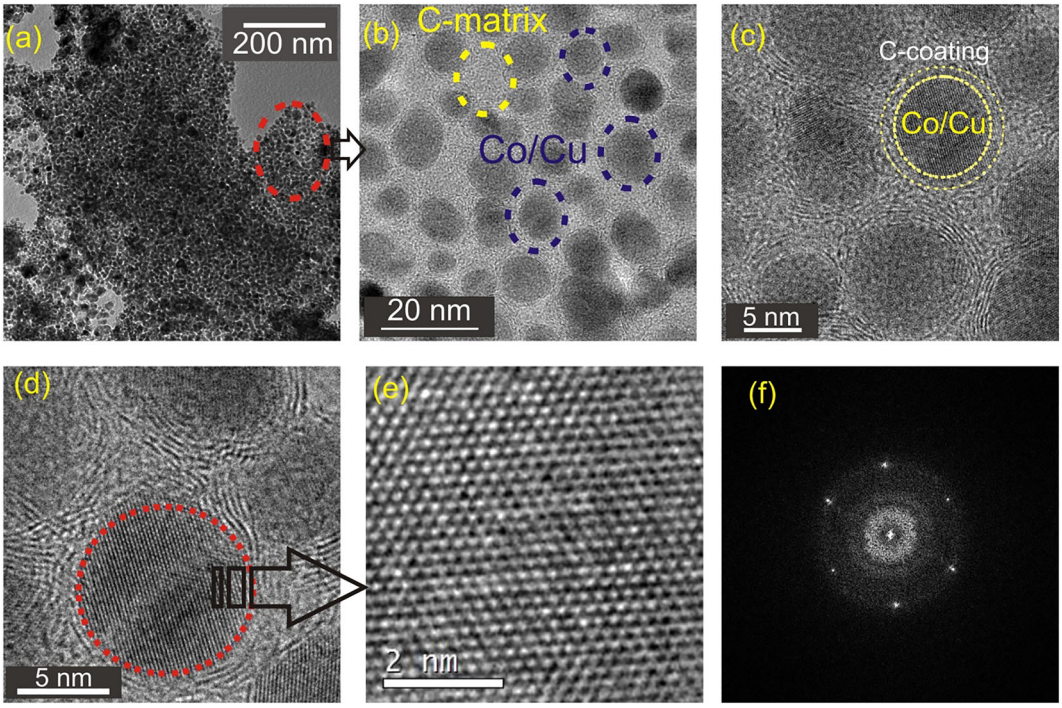


FIGURE 5 (a–e) Transmission electron microscopy (TEM) images of Cu/Co@NPC with different magnifications and (f) FFT diffractogram of Panel e. The yellow and dark blue regions in Panel b show the carbon matrix and Co/Cu crystalline phase at Cu/Co@NPC catalyst. The region with yellow short lines in Panel c shows the carbon coating around Co/Cu grains, and the periodic lattice formation was observed.

Co, cubic Fm3m			Cu, cubic Fm3m			From TEM-SAED
d (Å)	Ref. pl.	2θ	d (Å)	Ref. pl.	2θ	d (Å)
2.0467	111	44.216				2.029
			2.088	111	43.297	2.031
1.7723	200	51.522				1.908
			1.808	200	50.433	1.934
1.2532	220	75.853	1.278	220	74.13	
1.0688	311	92.224	1.09	311	89.931	

TABLE 1 The d-space, reflection plane, and 2θ values of Co (Fm3m) and Cu (Fe3m) species obtained from SAED measurements

10990739, 2023, 3, Downloaded from https://onlinelibrary.wiley.com/doi/10.1002/aoc.7017 by T C Inonu University, Wiley Online Library on [19/02/2023]. See the Terms and Conditions (https://onlinelibrary.wiley.com/terms-and-conditions) on Wiley Online Library for rules of use; OA articles are governed by the applicable Creative Commons License

In order to further study the porous structures of Cu/Co@aZIF and Cu/Co@NPC, N_2 adsorption–desorption tests were further investigated (Figure 6a). According to the adsorption isotherm, both the Cu/Co@aZIF and Cu/Co@NPC materials possessed Type II isotherms, which is attributed to their microporous and mainly mesoporous structures. The Brunauer–Emmett–Teller (BET) specific surface areas of Cu/Co@aZIF and Cu/Co@NPC were measured as 47.58 and 91 $m^2\ g^{-1}$, respectively. The pore size distributions and pore volumes were calculated using the Barrett–Joyner–Halenda (BJH) method, and it was found that Cu/Co@aZIF and Cu/Co@NPC had a broad pore size distribution between 1 and 20 nm (Figure 6b) and pore volumes of 0.198 and 0.34 $cm^3\ g^{-1}$, respectively. The average pore diameter (4 V/A by BET) of Cu/Co@aZIF and Cu/Co@NPC materials was found to be 3.7 and 6.1 nm, respectively.

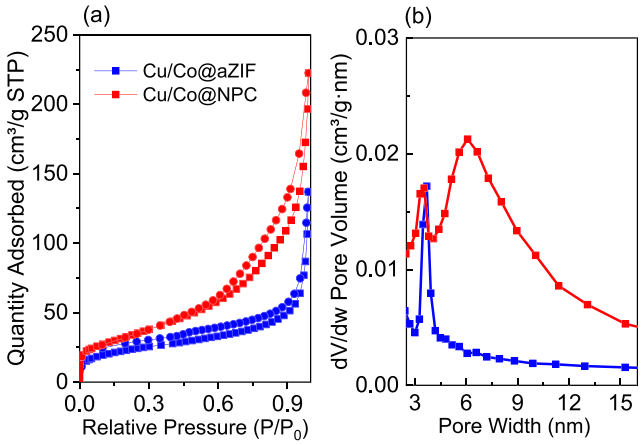


FIGURE 6 N_2 adsorption–desorption isotherms (a) and pore size distribution (b) of Cu/Co@aZIF and Cu/Co@NPC materials

To better understand the surface composition of the Cu/Co@NPC catalyst, X-ray photoelectron spectroscopy (XPS) measurement was performed (Figure 7). The elemental composition can be seen in Figure 7a, and the peaks around 284.5, 379.0, 778.3, 993.1, and 568.3 eV were assigned to C1s, N1s, Co2p, Cu2p, and O1s, respectively. The high-resolution XPS spectra of Cu2p (Figure 7b) possessed two main peaks at 932.8 and 952.6 eV, which ascribed to $Cu2p_{3/2}$ and $Cu2p_{1/2}$, respectively. The peaks at 932.8 and 934.7 eV ascribed to Cu(0) or Cu(I) and Cu(II) species,[36] which indicates that the Cu species were mainly Cu(0) and a minor proportion of Cu(II) was present. The high-resolution spectra of $Co2p_{3/2}$ and $Co2p_{1/2}$ (Figure 7c) showed characteristic peaks at 778.3, 779.9, 793.8, and 800.6 eV, corresponding to CoO_x or CoC_xN_y, Co-N_y, Co, and CoO, respectively.[40] In addition, the peak at 784.2 eV is defined as the satellite peak of the $Co3p_{1/2}$.

The N1s XPS spectrum is presented in Figure 7d. Three peaks at 398.1, 399.5, and 401.1 eV confirmed the existence of pyridinic-N, pyrrolic-N, and graphitic-N.[41]

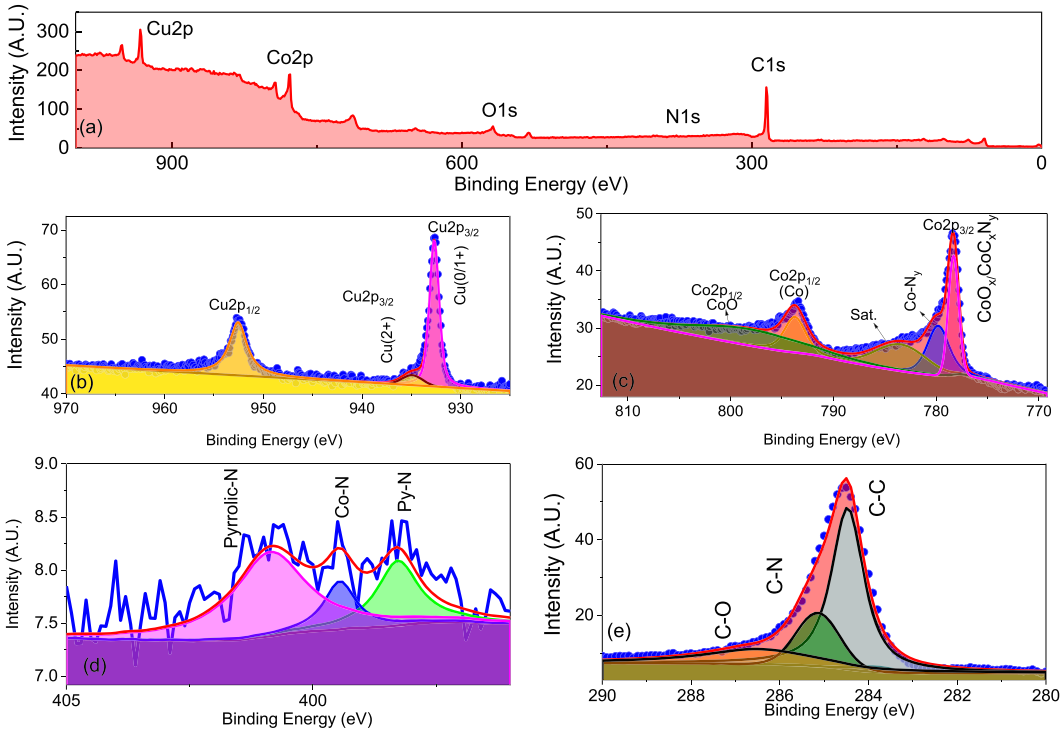


FIGURE 7 Full-scan X-ray photoelectron spectroscopy(XPS) spectra (a), Cu2p peak (b), Co2p peak (c), N1s peak (d), and C1s peak (e) for the Cu/Co@Nitrogen-doped porous carbon(NPC) catalyst

10990739, 2023, 3, Downloaded from https://onlinelibrary.wiley.com/doi/10.1002/aoc.7017 by T C Inonu University, Wiley Online Library on [19/02/2023]. See the Terms and Conditions (https://onlinelibrary.wiley.com/terms-and-conditions) on Wiley Online Library for rules of use; OA articles are governed by the applicable Creative Commons License

The XPS peaks at 284.5, 285.2, and 286.8 eV in the C1s spectrum are assigned to sp^2 hybridized C–C, sp^3 hybridized C–N, and O═C–O bonds (Figure 7e), respectively.[42]

3.2 | Catalytic studies

3.2.1 | Copper(I)-catalyzed Huisgen 1,3-dipolar cycloaddition of organic azides

We first investigated the catalytic performance of Cu/Co@NPC by studying the model reactions of benzyl chloride, sodium azide, and phenylacetylene in the presence of the Cu/Co@NPC catalyst in water for 1 h. Table 2 shows that the highest yield (99%) was achieved when the reaction was conducted at 80°C for 1 h using 4 mg of the Cu/Co@NPC catalyst (contains 0.001 mol% Cu and 0.0047 mol% Co) in a water solution (Table 2, entry 1). In addition, different alcohols, acetonitrile, and 1,4-dioxane were tested as solvents in the AAC reactions, and results showed that low yields (Table 2, entries 2–6) were obtained when reactions were carried out in different solvents instead of water. Another crucial parameter impacting product yield is catalyst concentration. To determine the optimum catalyst concentration, we conducted a reaction with a half catalyst concentration, and

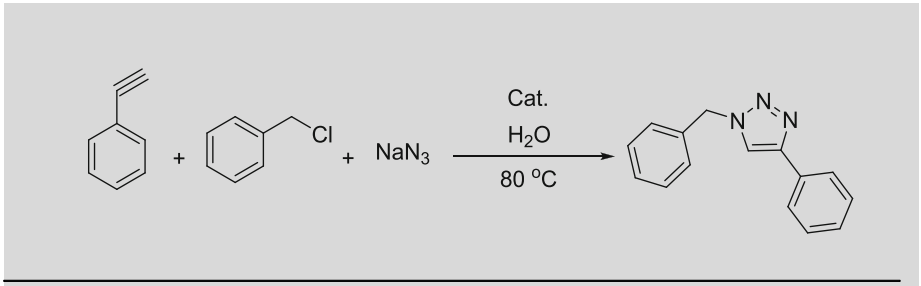


TABLE 2 Optimization of reaction conditions for AAC reaction[a]

Entry	Catalyst	Solvent	Yield (%)[b]
1	Cu/Co@NPC	H_2O	99
2		EtOH	37
3		MeOH	29
4		CH_3CN	34
5		*i*-PrOH	38
6		1,4-Dioxane	45
7[c]		H_2O	95
8[d]		H_2O	53
9[e]		H_2O	36
10[f]		H_2O	22
11[g]	Co@NPC	H_2O	18
12[h]	Cu/Co@aZIF	H_2O	69
13	CuCl (1 mol%)	H_2O	55
14	CuBr (1 mol%)	H_2O	70
15	Cu_2O (1 mol%)	H_2O	43
16	Cu $(OAc)_2$ (1 mol%)	H_2O	62
17	$CuSO_4$ (1 mol%)	H_2O	69

Abbreviations: AAC, azide-alkyne cycloaddition; ZIF, Zeolitic imidazolate framework; NPC, Nitrogen-doped porous carbon.

[a]Reaction conditions: benzyl chloride (1.0 mmol), sodium azide (1.0 mmol), phenylacetylene (1.2 mmol), H_2O (2 ml), 4 mg catalyst (0.001 mol% Cu, 0.0047 mol% Co), 80°C, 1 h.

[b]GC yields.

[c]Two milligrams of the Cu/Co@NPC catalyst (0.0005 mol% Cu, 0.00235 mol% Co) used.

[d]One milligram of the Cu/Co@NPC catalyst (0.00025 mol% Cu, 0.001175 mol% Co) used.

[e]Twenty-five degrees Celsius, 6 h.

[f]Fifty degrees Celsius, 1 h.

[g]Four milligrams of the Co@NPC catalyst contains 0.004 mol% Co.

[h]Four milligrams of the Cu/Co@aZIF catalyst (0.0006 mol% Cu and 0.0027 mol% Co).

10990739, 2023, 3, Downloaded from https://onlinelibrary.wiley.com/doi/10.1002/aoc.7017 by T C Inonu University, Wiley Online Library on [19/02/2023]. See the Terms and Conditions (https://onlinelibrary.wiley.com/terms-and-conditions) on Wiley Online Library for rules of use; OA articles are governed by the applicable Creative Commons License

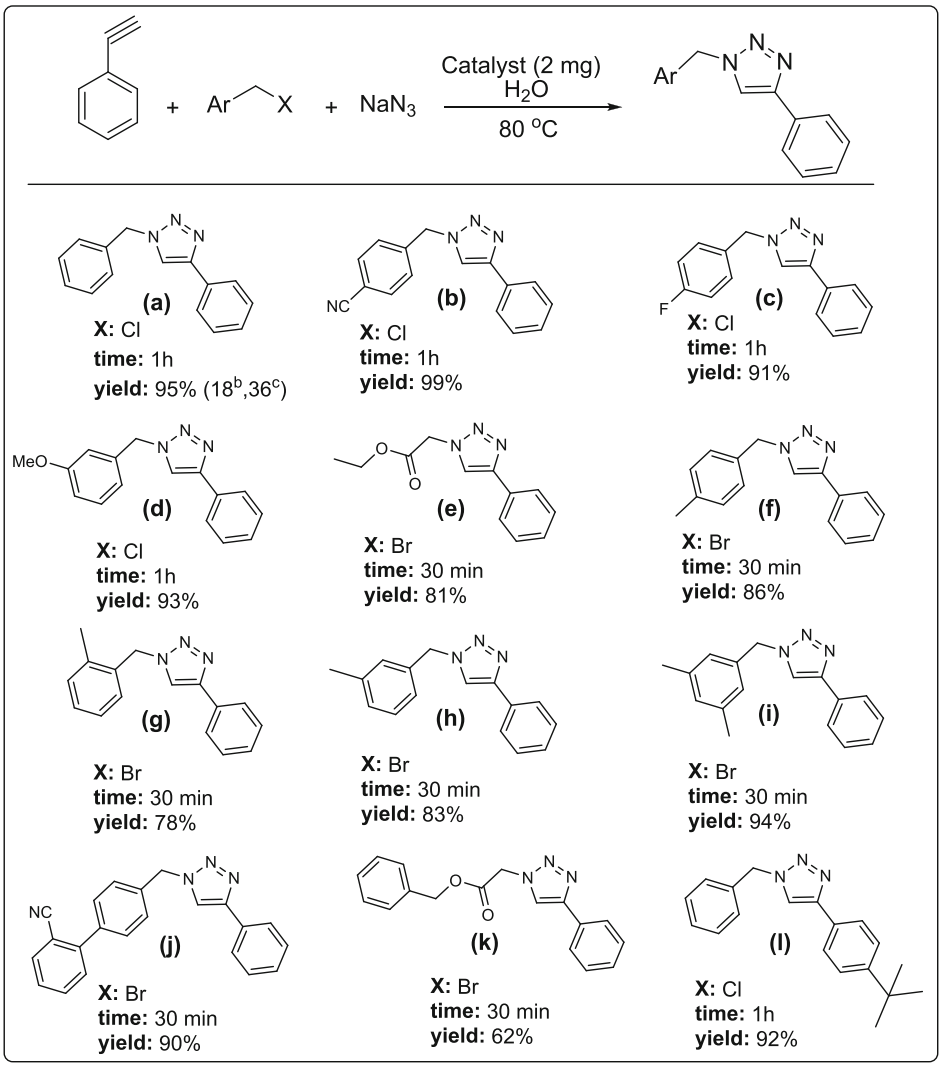
the results revealed that the yield was not significantly decreased (Table 2, entry 7). However, when the catalyst concentration dropped to 1 mg, a 53% yield was obtained (Table 2, entry 8). Because the results we got with 2 mg of catalyst were quite good, we decided that this catalyst concentration is the ideal amount for the rest of the catalytic reactions.

Product yields are also affected by the reaction temperature. The reaction performed at lower temperatures resulted in a lower yield than the reaction performed at 80°C (Table 2, entries 9 and 10). In contrast, the heterogeneous Co@NPC catalyst, which contains 0.004 mol% Co, provided a product with only an 18% yield (Table 2, entry 11). As a result of this finding, the significance of Cu metal in AAC reactions was highlighted once more.

The use of the Cu/Co@aZIF catalyst for the AAC reaction was also investigated to make a comparison. The yield of the reaction catalyzed by Cu/Co@aZIF is quite encouraging (Table 2, entry 12). However, using an external magnet to separate the catalyst from the reaction medium is difficult. For the catalyst's reusability, this is a crucial point. In addition to this, the lower surface area and pore volume of the Cu/Co@aZIF catalyst result in a lower yield compared with the yield using the Cu/Co@NPC catalyst. These findings suggest that producing nano-sized Cu and Co particles embedded in a carbon network increases catalytic activity through increased permeability of the substrate and a faster transfer of electrons from donor to acceptor.

Yields of 55% and 70% were obtained using CuCl and CuBr catalyses, respectively, reflecting the reduced

TABLE 3 Cu/Co@NPC-catalyzed AAC reaction of phenylacetylene and organic halides[a]



Abbreviations: AAC, azide-alkyne cycloaddition.

[a]Reaction conditions: 80°C, 1 h, H_2O, 2 mg Cu/Co@NPC (0.0005 mol% Cu, 0.00235 mol% Co).

[b]Eighty degrees Celsius, 1 h, H_2O, 4 mg Co@NPC (0.004 mol% Co).

[c]Twenty-five degrees Celsius, 6 h, H_2O, 4 mg Cu/Co@NPC (0.001 mol% Cu, 0.0047 mol% Co).

10990739, 2023, 3, Downloaded from https://onlinelibrary.wiley.com/doi/10.1002/aoc.7017 by T C Inonu University, Wiley Online Library on [19/02/2023]. See the Terms and Conditions (https://onlinelibrary.wiley.com/terms-and-conditions) on Wiley Online Library for rules of use; OA articles are governed by the applicable Creative Commons License

efficiency of these catalysts (Table 2, entries 13 and 14). Table 2 shows that the yields for the AAC reaction when using Cu_2O, $Cu(OAc)_2$, and $CuSO_4$ as catalysts were only 43%, 62%, and 69%, respectively. Based on these findings, it appears that the Cu/Co@NPC nanocatalyst possesses excellent catalytic activity.

As soon as the optimum conditions for the AAC reaction were determined, the substrate scope was examined (Table 2). The reaction of phenylacetylene with various benzyl halides gave the relevant products in high yields (Table 3). From Table 3, it is clear that the reactivities of substituted or unsubstituted benzyl halides with either electron-donating groups, such as 2-methylbenzyl chloride, or electron-withdrawing groups, such as 4-fluorobenzyl chloride, are very similar to each other. The reactivity of benzyl bromide was, however, increased by a factor of 1 over that of benzyl chloride. This demonstrates that the reaction yield is directly affected by the type of halides used on Ar-X. Furthermore, steric hindrance does not substantially impact the reaction yield. For instance, the reaction of *p*-methylbenzyl bromide resulted in an 86% yield, whereas *m*-methylbenzyl bromide and *o*-methylbenzyl bromide yielded 78% and 83%, respectively (Table 3). Good to high yields (62%–81%) were obtained in the first 30 min of the AAC reaction of ethyl bromoacetate and benzyl bromoacetate with phenylacetylene. Obtaining these products with the catalytic system that we have developed is another indicator of the efficiency of the catalyst. However, a high yield (92%) was also obtained in the cycloaddition of benzyl chloride with 4-*tert*-buthylacetylene. The results show that the Cu/Co@NPC nanocatalyst was able to speed up the AAC reaction of electron-donated alkyne with benzyl chlorides.

3.2.2 | Recyclability studies of the magnetic Cu/Co@NPC nanocatalyst

The recyclability of the magnetic Cu/Co@NPC nanocatalyst was investigated for 1 h using the reaction of phenylacetylene, benzyl chloride, and sodium azide. After five cycles of AAC reactions, the catalytic activity decreased by 22%, as determined by the findings (Figure 8). In Cu leaching experiments, very little or no Cu metal was detected in the solution according to Inductively coupled plasma mass spectrometry (ICP-MS) analysis. The Cu percentage of the five-times-reused Cu/Co@NPC was measured to be 16.5 wt%, indicating low Cu leaching. SEM and TEM analyses of the five-times-used Cu/Co@NPC nanocatalyst indicated that the skeleton structure, morphology, and Cu and Co contents of the catalyst remained almost identical to the original structure (Figures S1 and S2).

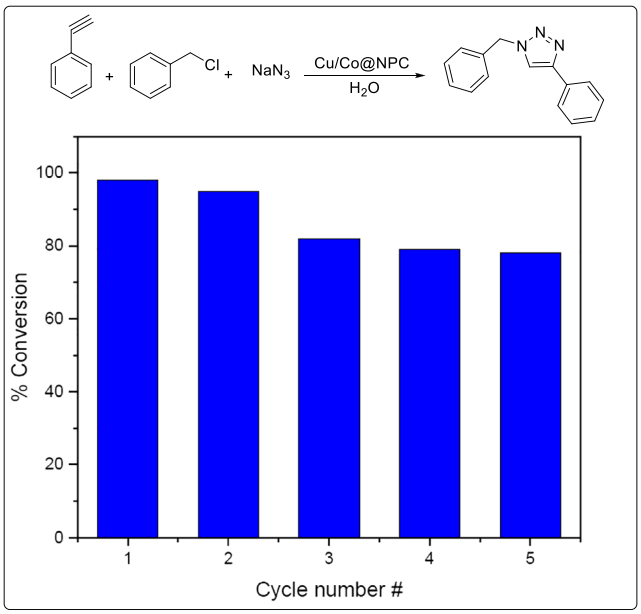


FIGURE 8 Recyclability of the Cu/Co@Nitrogen-doped porous carbon(NPC) (2 mg) catalyst for the azide-alkyne cycloaddition (AAC) reaction in water. (a) The click reaction between benzyl chloride (1 mmol), phenylacetylene (1 mmol), and sodium azide (1 mmol) under air at 80°C

A hot-filtration test was conducted to demonstrate that heterogeneous Cu doped into a carbon network catalyzes the CuAAC process. The benzyl chloride, sodium azide, and phenylacetylene reactions were initiated. At 30 min of reaction, before all substrates were totally depleted, an external magnet was used to extract the catalyst (Figure 9), and 100 µl of filtrate was taken for the Gas chromatography(GC) analysis. The remaining catalyst-free filtrate was permitted to react under the same reaction conditions as the first filtrate. The hot-filtration test revealed an additional 3% conversion after 30 min, indicating that the process is catalyzed by a Cu/Co@NPC nanocatalyst.

Figure 9 shows the solid-state and liquid-state magnetic responses of the catalyst while an external magnet is applied. When the catalyst is in a solid state and an external magnet is introduced close to it, the Co and Cu nanoparticles in the catalyst provide a very strong magnetic response. The catalyst in the water does eventually collect around the magnet, but it takes around 5 min. Thanks to this superior magnetic response of the catalyst, it paves the way for the catalyst to be easily separated from the catalytic system and used again.

Figure 10 depicts a potential reaction pathway for the AAC reaction[43] catalyzed by Cu/Co@NPC. To begin, the alkyne reacts with the magnetic Cu/Co@NPC to produce NPC@CoCu-acetylide. Then, the azide's nucleophilic assaults on NPC@CoCu-acetylide generate an

10990739, 2023, 3, Downloaded from https://onlinelibrary.wiley.com/doi/10.1002/aoc.7017 by T C Inonu University, Wiley Online Library on [19/02/2023]. See the Terms and Conditions (https://onlinelibrary.wiley.com/terms-and-conditions) on Wiley Online Library for rules of use; OA articles are governed by the applicable Creative Commons License

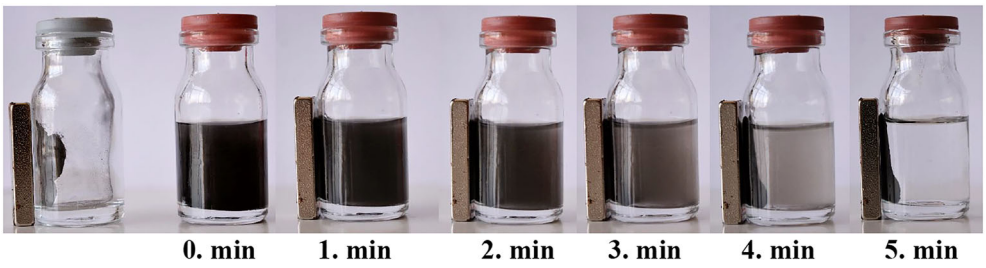


FIGURE 9 The magnetic separation of Cu/Co@NPC by an external magnet in water

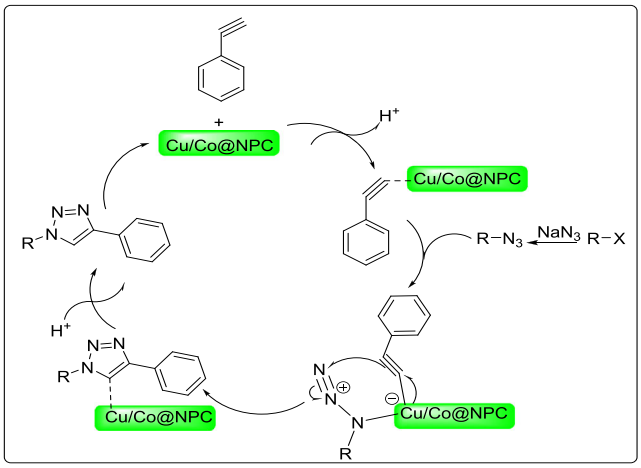


FIGURE 10 The proposed catalytic mechanism for the azide-alkyne cycloaddition (AAC) reaction catalyzed by Cu/Co@NPC

ionic copper complex. This ionic copper complex undergoes intramolecular rearrangement and turns into a metallacycle intermediate. After ring contraction of the metallacycle intermediate, a copper-triazolide complex forms. Once and for all, the copper-triazolide complex receives a proton for the production of substituted triazole and renewal of the active magnetic Cu/Co@NPC nanocatalyst.

The catalytic activity of the Cu/Co@NPC in the AAC reaction was compared in Table 4 with similar catalysts synthesized from MOF derivatives in the literature. The advantages of the AAC catalytic system catalyzed by Cu/Co@NPC over other MOF-derived catalysts are as follows: (1) *requires less catalyst concentration*; (2) *shorter reaction time*; (3) *high efficiency with chlorinated substrates*; and (4) *high reusability*. To the best of our knowledge, the Cu/Co@NPC is the only catalyst that combines

TABLE 4 Comparison of AAC reaction between benzyl azide and phenylacetylene using Cu catalysts in the recent pieces of literature

Cu-MOF catalyst	Reaction conditions (amount of catalyst, amount of benzyl azide, solvent, temperature, time, and additive)	Yield (%)	Ref.
Cu/Co@NPC	5×10^{-4} mol%, 1 mmol, H_2O, 80°C, 1 h	95	This work
$Cu_4L(SiW_{12}O_{40})\cdot 6H_2O\cdot 2DMF$	30 mg, 1 mmol, MeOH, 80°C, 12 h, amyl acetate	99	[44]
Cu-MOF	5 mol%, 0.37 mmol, EtOH/H_2O, rt, 12 h	95	[45]
Cu25%/ZIF-8	5 mol% catalyst, 1 mmol, EtOH, 70°C, 3 h	99	[46]
Cu(I)-MOF	1 mol% (based on Cu element), 1 mmol, DMF/DMSO, 60°C, 4 h	99	[47]
CuI@UiO-67-IM	2 mol%, 1 mmol, H_2O, 80°C, 2 h	89	[48]
Cu-MOF	0.25 mol%, 1 mmol, neat, 50°C, 2.5 h	94	[49]
Copper-MOF	0.1 mol%, 1 mmol, EtOH, 70°C, 1 h	99	[50]
Cu-MOF	10 mol%, 1 mmol, H_2O/MeOH, 70°C, 2 h, sodium ascorbate, K_2CO_3	93	[51]
Cu(BTC)-MOF	10 mg, 1.6 mmol, MeOH, rt, 16 h	88	[52]
$Cu(INA)_2$-MOF	1 mol%, 0.5 mmol, solvent free, 80°C, 4 min	95	[53]
MOF-2	1 mol%, 0.1 mmol, H_2O/CH_3CN, rt (WLED [24 W]), 8 h	45	[54]

Abbreviations: MOF, metal–organic framework; WLED, white light-emitting diode; NPC, Nitrogen-doped porous carbon; DMF, Dimethylformamid; ZIF, Zeolitic imidazolate framework; BTC, benzene-1,3,5-tricarboxylic acid; INA, isonicotinate ion.

10990739, 2023, 3, Downloaded from https://onlinelibrary.wiley.com/doi/10.1002/aoc.7017 by T C Inonu University, Wiley Online Library on [19/02/2023]. See the Terms and Conditions (https://onlinelibrary.wiley.com/terms-and-conditions) on Wiley Online Library for rules of use; OA articles are governed by the applicable Creative Commons License

the aforementioned superior properties and demonstrated the best catalytic performance among the catalysts reported thus far.

3.2.3 | Reduction of 4-NP

Figure 11 depicts the catalytic transformation of nitrophenols to aminophenols by a Cu/Co@NPC nanocatalyst in the presence of a high concentration of $NaBH_4$. MNPs embedded in support materials may promote the transmission of electrons from $NaBH_4$ to nitrophenol.[34] According to Figure 11a, the absorbance of 4-NP at 316.6 nm shifts to 400 nm upon the addition of $NaBH_4$.

Because of the increase in pH value caused by the addition of $NaBH_4$, this chemical transformation causes the solution's color to transform from pale yellow to bright yellow. The observation of these physical and chemical changes is evidence of the formation of 4-nitrophenolate. It is understood that 4-nitrophenolate can remain in a catalyst-free environment for 15 min without undergoing any structural chemical changes (Figure S3b). After this result, supported by the literature, 4-NP cannot be reduced to 4-AP in the absence of a catalyst.[25] When 0.5 mg of the Cu/Co@NPC nanocatalyst was introduced into an aqueous solution of 4-nitrophenolate, the solution turned colorless until the end of the reaction. However, the absorption peak of 4-nitrophenolate at 400 nm decreased rapidly, and the

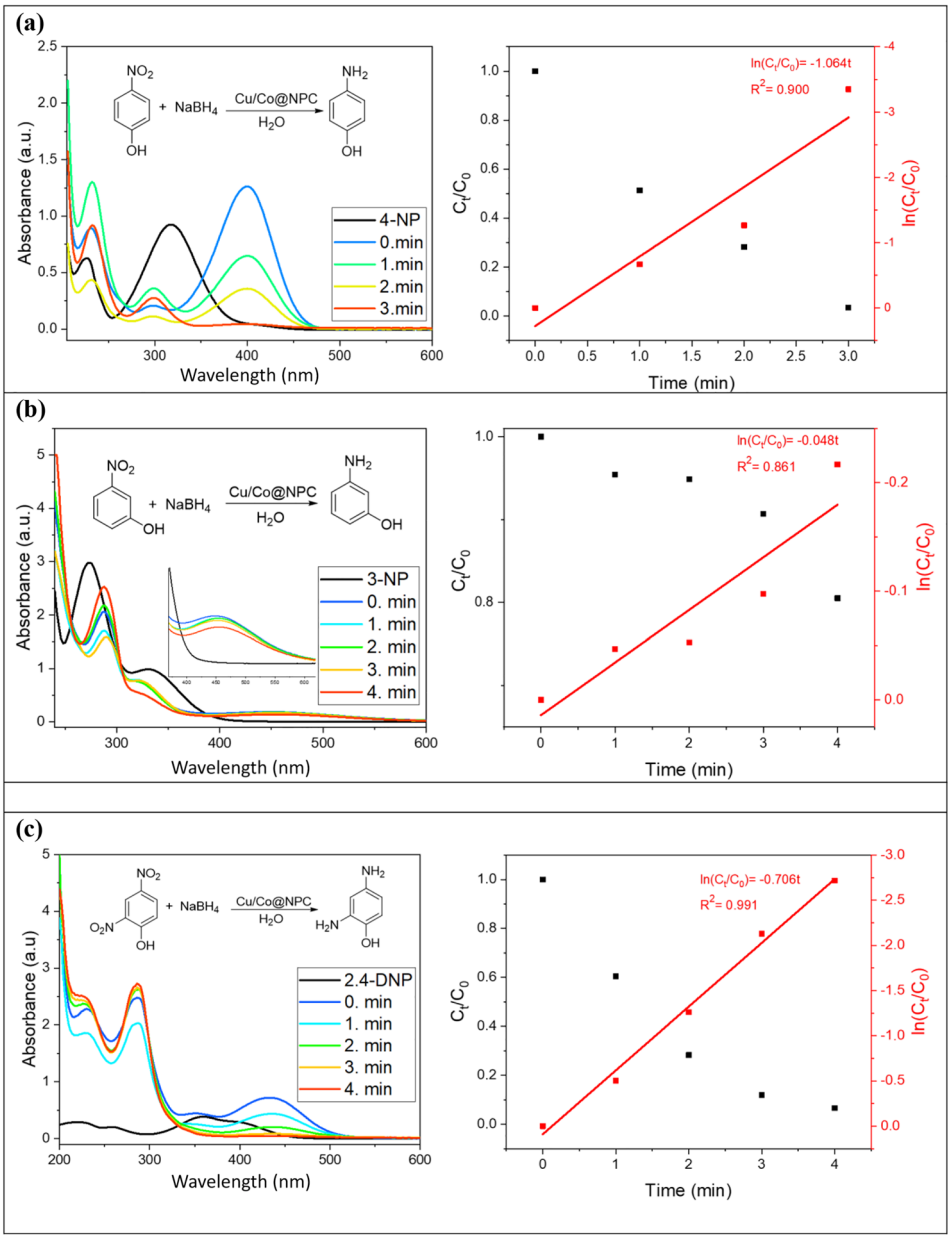


FIGURE 11 Curves of conversion versus time and the relationship between $\ln(C_t/C_0)$ and reaction time (t) for reduction of the 4-nitrophenol (4-NP) (a), 3-nitrophenol(3-NP) (b), and 2,4-dinitrophenol(2,4-DNP) over Cu/Co@Nitrogen-doped porous carbon(NPC) (c)

10990739, 2023, 3, Downloaded from https://onlinelibrary.wiley.com/doi/10.1002/aoc.7017 by T C Inonu University, Wiley Online Library on [19/02/2023]. See the Terms and Conditions (https://onlinelibrary.wiley.com/terms-and-conditions) on Wiley Online Library for rules of use; OA articles are governed by the applicable Creative Commons License

new absorption peak of 4-AP appeared at 300 nm (Figure 11a). The reaction is carried out in a quartz sleeve in an ultrasonic bath at room temperature and monitored with a UV–Vis spectrometer by taking measurements at certain time intervals until the corresponding absorption peaks disappear. Figure 11b,c shows the plots of absorbance versus wavelength at different times for the reduction reactions of 3-nitrophenol and 2,4-dinitrophenol, respectively. The aqueous solutions of 3-NP and 2,4-DNP showed maximum absorbances at 274.0 and 357.5 nm, respectively. The introduction of an aqueous solution of $NaBH_4$ with 3-NP and 2,4-DNP led to shifts in the absorbances to 410 and 437 nm, respectively. After the Cu/Co@NPC catalyst was introduced, the peaks at 410 and 437 nm decreased rapidly, whereas increasing new peaks appeared at 289 and 290.6 nm (Figure 11b,c), attributed to the formation of related aminophenol derivatives (Figure 11b,c).

Through the kinetic analyses, plots of the C_t/C_0 as a function of time and the kinetic curves of each reaction were examined (Figure 11a–c). Because the concentration of $NaBH_4$ was significantly higher than that of nitrophenols, it is reasonable to assume that the quantity of $NaBH_4$ does not vary during the reaction. Because of a pseudo-first-order reaction, the rate of the reaction probably only depends on the concentration of nitrophenol derivatives. The ratio of the concentrations C_t of the Nitrophenol(NP) derivatives at time t to their initial values at C_0 at $t = 0$ follows directly from the ratios of the corresponding absorbances A_t/A_0 (A = absorbances at 400, 410, and 437 nm for 4-nitrophenolate, 3-nitrophenolate, and 2,4-dinitrophenolate, respectively), so the kinetic equations for the reductions of (NP) derivatives can be written as

$$dC_t/dt = -k_{app}C_t \text{ or } \ln(C_t/C_0) = \ln(A_t/A_0) = -k_{app}C_t$$

The slopes were applied to the plot of $\ln(C_t/C_0)$ versus time to provide pseudo-first-order rate constants. The rate constants (K_{app}) of Cu/Co@NPC were found to be 1.064, 0.048, and 0.706 min^{-1} for 4-NP, 3-NP, and 2,4-DNP (Figure 11a–c). In our previous work,[8] K_{app} and the mass-normalized rate constants K_m ($K_m = K_{app}/m_{cat}$) (min^{-1} mg^{-1}) were calculated as 0.122 min^{-1} and 0.0406 min^{-1} mg^{-1}, respectively, for 4-NP in the presence of the Co@NPC@ZIF-12 catalyst. In this work, the K_m was calculated as 0.594, 0.0268, and 0.394 min^{-1} mg^{-1} for 4-NP, 3-NP, and 2,4-DNP, respectively, over the Cu/Co@NPC catalyst. From these results, the activity of Cu nanoparticles in the reduction of nitrophenols is quite clear, and it is thought that it creates a synergistic effect with cobalt nanoparticles. Further, the Cu/Co@NPC catalyst's activity against these substrates was evaluated using turnover frequency (TOF): (mol NP/mol catalyst)/unit reaction time. After calculations, TOF values of 18.3, 29.4, and 29.4 h^{-1} were found for 4-NP, 3-NP, and 2,4-DNP, respectively (conditions and reagent amounts used in TOF calculations: $n_{cat(Cu/Co)}$: 1469×10^{-5}; n_{NP}: 7.18×10^{-5}; per unit reaction time: 16, 10, and 10 m for 4-NP, 3-NP, and 2,4-DNP, respectively; $Mw_{Cu/Co}$: 122.47 mol g^{-1}; the reaction was carried out in a round-bottom balloon with stirring for the specified times under air).

When comparing the mesomeric effect with the inductive effect, the mesomeric effect is more prominent in the nitro group. The NO_2 group at the *o*- and *p*-positions withdraws the electron of the O–H bond towards it by a stronger mesomeric effect, whereas the NO_2 group at the *m*-position withdraws the electron of the O–H bond by a weaker inductive effect. Thus, the electron density of *o*- and *p*-nitro nitrophenols increases, leading to more acidic nitrophenols than *m*-nitrophenol. Because nitrophenols undergo a nucleophilic reduction reaction, the lower electron density of their nitro groups is directly boosting their reactivity. Therefore, low electron density on nitro groups creates an accelerating effect on reduction. The fact that *m*-nitrophenol is the most active substrate is consistent with this information.

The literature suggests that Co nanoparticles encased in a carbon matrix can convert 4-NP to 4-AP. According to the research of Zhao and Zhao, the catalytic activity of nanoparticles is due to the Co nanoparticle cores.[55] This finding suggests that Cu and Co, where the synergistic effect plays a crucial role, are responsible for the high catalytic activity of the Cu/Co@NPC nanocatalyst, in agreement with other reports in the literature.[56–59] The synergy between Cu and Co nanoparticles, or the relative contribution of each metal to the reaction, was investigated in a separate experiment using Co@NPC. The ZIF-derived Co@NPC catalyst (2 mg catalyst, 0.002 mol% Co) demonstrated 100% conversions in 18 min for the reduction of 4-NP, 15 min for the reduction of 3-NP, and 18 min for the reduction of 2,4-DNP (ICP-MS result: 61.25 wt% Co nanoparticles) (Figure S3a). As evidenced by the results, the Co@NPC catalyst exhibited less catalytic activity than Cu/Co@NPC. We believe that copper is responsible for this difference in catalytic activity. The recyclability of the Cu/Co@NPC nanocatalyst in reducing 4-NP to 4-AP was examined (Figure 12), and results showed that the Cu/Co@NPC nanocatalyst works very well even after five consecutive runs.

As a result, most research on nitrophenol substrate reduction has been on 4-NP, whereas 3-NP reduction has

10990739, 2023, 3, Downloaded from https://onlinelibrary.wiley.com/doi/10.1002/aoc.7017 by T C Inonu University, Wiley Online Library on [19/02/2023]. See the Terms and Conditions (https://onlinelibrary.wiley.com/terms-and-conditions) on Wiley Online Library for rules of use; OA articles are governed by the applicable Creative Commons License

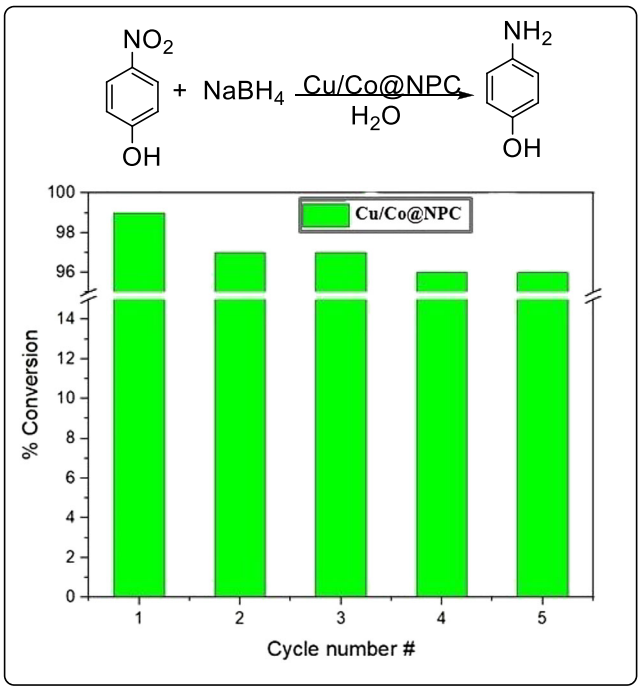


FIGURE 12 The recyclability of the Cu/Co@NPC nanocatalyst in reducing 4-NP to 4-AP

received less attention. This motivates us to look into the Cu/Co@NPC nanocatalyst's performance in the reduction of 4-NP and make a quick comparison with commercial Pd/C and the existing literature.

According to the research done by Zhang et al., the TOF value for the commercial Pd/C catalyst is 62 h^{-1}. The TOF value of the Cu/Co@NPC nanocatalyst was calculated as 18.3 h^{-1}, which is lower than the commercial Pd/C catalyst and some of those previously reported catalysts (Table 5).[2,35,36,60–71]

However, the nanocatalyst discussed here outperforms conventional catalysts in a shorter time frame, under air, and with a smaller catalyst load than commercial Pd/C catalysts and catalysts reported in the literature. The carbon matrix hosting Cu and Co nanoparticles may be responsible for the increased catalytic activity of the Cu/Co@NPC nanocatalyst by aiding the mass transfer of the nitro compound.

In this part of the research, we found that utilizing Cu and Co nanoparticles encased in an aZIF-synthesized carbon matrix might be used instead of the commercial Pd/C catalyst because of the high price of palladium and the reaction conditions, such as the H_2 atmosphere, which are specific to this catalyst. Among the catalysts listed in Table 5, the Cu/Co@NPC nanocatalyst is clearly the most cost-effective option.

TABLE 5 Literature data comparisons for the reduction of 4-nitrophenol

Catalyst	Reaction conditions (4-NP, $NaBH_4$, Cat., T, TOF, and K_m)	Ref.
Cu/Co@CF	0.1 mM, 0.2 M, 0.05 mg, 25°C, 102.44 min^{-1} mg^{-1}	[2]
Co@NC	5 mM, 5.0 mM, 0.02 mg, 25°C, 45 h^{-1}, 51.2 min^{-1} mg^{-1}	[35]
Cu/Co@NCF	0.1 mM, 0.2 M, 0.05 mg, 25°C, 435.6 h^{-1}, 83.18 min^{-1} mg^{-1}	[36]
Pt nanotubes	0.09 mM, 0.1 M, 0.09 mM, 25°C, 13.3 min^{-1} mg^{-1}	[60]
PdPt nanotubes	0.09 mM, 0.1 M, 0.09 mM, 25°C, 33.3 min^{-1} mg^{-1}	[60]
Ag nanodendrites	0.1 mM, 0.3 M, 2 mg, 25°C, 0.2 min^{-1} mg^{-1}	[61]
AuNPs/r-CD	1 mM, 0.6 M, 0.4 mM, 25°C, 0.1 min^{-1} mg^{-1}	[62]
Pd-Ni/rGO	5 mM, 0.03 M, 0.2 mg, 25°C, 0.8 min^{-1} mg^{-1}	[63]
NiO/CuO	0.1 mM, 0.1 mM, 0.005 mg, 25°C, 30.1 min^{-1} mg^{-1}	[64]
CP-1000	0.1 M, 0.02 mM, 0.01 mg, 25°C, 1.536 h^{-1}, 26.24 min^{-1} mg^{-1}	[65]
Cu-based MOFs	0.4 mM, 0.1 M, 2 mg, 25°C, 0.425 min^{-1} mg^{-1}	[66]
CoOx/CN-500	0.4 mM, 0.2 M, 2 mg, 25°C, 0.126 min^{-1} mg^{-1}	[67]
Pd@MIL-100 (Fe)	0.676 mM, 35 M, 0.525 mg, 25°C, 2112 h^{-1}, 0.0123 min^{-1} mg^{-1}	[68]
Pd@ZIF-8	7.2 mM, 0.7 M, 10 mg, 25°C, 792 h^{-1}	[69]
Fe_3O_4@M/MIL-100 (Fe)	1.39 M, 0.1 M, 0.025 mg, 25°C, 1332 h^{-1}	[70]
Pd/C	0.02 M, under H_2 atm., 10 mg, 25°C, 62 h^{-1}	[71]
Cu/Co@NPC[a]	3.59 mM, 0.2 M, 1.79 mg CuCo, 25°C, 18.3 h^{-1}, 0.116 min^{-1} mg^{-1}	This work

Abbreviations: MOF, metal–organic framework; TOF, turnover frequency CF, Carbon Framework; NC, N-doped carbon framework; rCD, reductive carbon dots; rGO, reduced graphene oxide; ZIF, Zeolitic imidazolate framework; NPC, Nitrogen-doped porous carbon.
[a]K_{app} was calculated as 0.208 min^{-1}.

4 | CONCLUSIONS

To generate a magnetic Cu/Co@NPC nanocatalyst, an aZIF-based porous carbon containing Cu and Co nanoparticles was devised and synthesized successfully via

10990739, 2023, 3, Downloaded from https://onlinelibrary.wiley.com/doi/10.1002/aoc.7017 by T C Inonu University, Wiley Online Library on [19/02/2023]. See the Terms and Conditions (https://onlinelibrary.wiley.com/terms-and-conditions) on Wiley Online Library for rules of use; OA articles are governed by the applicable Creative Commons License

the pyrolysis of Cu/Co@aZIF. The magnetic Cu/Co@NPC nanocatalyst showed superior catalytic activity, high stability, and good reusability for AAC and reduction reaction of nitrophenol (RRN) reactions in water and under atmospheric conditions. This work could provide an efficient way for the synthesis of substituted triazoles and aminophenols via the AAC and RRN reactions, respectively, catalyzed by an ultra-efficient magnetic Cu/Co@NPC heterogeneous catalyst. High stability with low catalyst loading is the most important feature of the AAC and RRN reaction catalytic systems.

ACKNOWLEDGMENTS

The İnönü University Research Council partially supported the study through project number FCD-2021-2557.

CONFLICT OF INTEREST

The authors declare that they have no known competing financial interests or personal relationships that could have appeared to influence the work reported in this paper.

AUTHOR CONTRIBUTIONS

Nesrin Buğday: Data curation; formal analysis; investigation; methodology; project administration; visualization; writing – original draft; writing – review and editing. **Sedat Yaşar:** Data curation; formal analysis; investigation; methodology; project administration; resources; supervision; visualization; writing – original draft; writing – review and editing. **Serdar Altin:** Data curation; formal analysis; methodology; validation; writing – original draft; writing – review and editing. **Ozgur Duygulu:** Formal analysis; methodology; visualization; writing – original draft; writing – review and editing. **Yunus Önal:** Methodology; writing – original draft; writing – review and editing.

DATA AVAILABILITY STATEMENT

The data that support the findings of this study are available from the corresponding author upon reasonable request.

ORCID

Nesrin Buğday https://orcid.org/0000-0002-3882-035X
Sedat Yaşar https://orcid.org/0000-0001-7285-2761
Serdar Altin https://orcid.org/0000-0002-4590-907X
Ozgur Duygulu https://orcid.org/0000-0001-8646-0363
Yunus Önal https://orcid.org/0000-0001-6342-6816

REFERENCES

[1] H. Wang, L. Wei, J. Liu, J. Shen, *Int. J. Hydrog. Energy* **2020**, *45*, 4481.
[2] Y. Zhang, C. Chu, Y. Xu, Z. Ma, H. Han, *Colloids Surf. A Physicochem. Eng.* **2022**, *641*, 128477.
[3] S.-N. Zhao, X.-Z. Song, S.-Y. Song, H.-J. Zhang, *Coord. Chem. Rev.* **2017**, *337*, 80.
[4] Y. S. Wei, M. Zhang, R. Zou, Q. Xu, *Chem. Rev.* **2020**, *120*, 12089.
[5] Y. Wu, X. Wang, K. O. Kirlikovali, X. Gong, A. Atilgan, K. Ma, N. M. Schweitzer, N. C. Gianneschi, Z. Li, X. Zhang, O. K. Farha, *Angew. Chem.* **2022**, *134*, e202117528.
[6] M. Qiu, T. Guo, R. Xi, D. Li, X. Qi, *Appl. Catal. A* **2020**, *602*, 117719.
[7] K. O. Kirlikovali, Z. Chen, T. Islamoglu, J. T. Hupp, O. K. Farha, *ACS Appl. Mater. Interfaces* **2020**, *12*, 14702.
[8] N. Buğday, S. Altın, S. Yaşar, *Appl. Organomet. Chem.* **2022**, *36*, e6797.
[9] N. Buğday, S. Altın, S. Yaşar, *Appl. Organomet. Chem.* **2021**, e6403.
[10] M. Maffei, G. Giacoia, R. Mancuso, B. Gabriele, E. Motti, M. Costa, N. Della Ca, *J. Mol. Catal. A Chem.* **2017**, *426*, 435.
[11] S. S. Dias, M. V. Kirillova, V. André, J. Kłak, A. M. Kirillov, *Inorg. Chem.* **2015**, *54*, 5204.
[12] F. Alonso, Y. Moglie, G. Radivoy, M. Yus, *Adv. Synth. Catal.* **2010**, *352*, 3208.
[13] M. Meldal, C. W. Tornøe, *Chem. Rev.* **2008**, *108*, 2952.
[14] The Nobel Prize in Chemistry, **2022**, https://www.nobelprize.org/prizes/chemistry/2022/press-release/
[15] B. Mondal, M. Kundu, S. P. Mandal, R. Saha, U. K. Roy, A. Roychowdhury, D. Das, *ACS Omega* **2019**, *4*, 13845.
[16] F. Wang, Y. Zhang, Z. Liu, Z. Du, L. Zhang, J. Ren, X. Qu, *Angew. Chem. Int. Ed.* **2019**, *58*, 6987.
[17] Y. Zhou, Y. Yu, D. Ma, A. C. Foucher, L. Xiong, J. Zhang, E. A. Stach, Q. Yue, Y. Kang, *ACS Catal.* **2020**, *11*, 74.
[18] Y. Tang, R. Liu, S. Liu, B. Zheng, Y. Lu, R. Fu, D. Wu, M. Zhang, M. Rong, *Carbon* **2019**, *141*, 704.
[19] L. N. Chen, H. Q. Li, M. W. Yan, C. F. Yuan, W. W. Zhan, Y. Q. Jiang, Z. X. Xie, Q. Kuang, L. S. Zheng, *Small* **2017**, *13*, 1700683.
[20] D. Liu, M. Li, X. Li, F. Ren, P. Sun, L. Zhou, *Chem. Eng. J.* **2020**, *387*, 124008.
[21] G. Vilé, G. Di Liberto, S. Tosoni, A. Sivo, V. Ruta, M. Nachtegaal, A. H. Clark, S. Agnoli, Y. Zou, A. Savateev, M. Antonietti, *ACS Catal.* **2022**, *12*, 2947.
[22] P. Shiri, J. Aboonajmi, *Beilstein J. Org. Chem.* **2020**, *16*, 551.
[23] N. Takahashi, T. Nakai, Y. Satoh, Y. Katoh, *Water Res.* **1994**, *28*, 1563.
[24] J. Kiwi, C. Pulgarin, P. Peringer, *Appl. Catal. Environ.* **1994**, *3*, 335.
[25] Z. Hasan, D. W. Cho, C. M. Chon, K. Yoon, H. Song, *Chem. Eng. J.* **2016**, *298*, 183.
[26] W. Zhang, X. Xiao, T. An, Z. Song, J. Fu, G. Sheng, M. Cui, *J. Chem. Technol. Biotechnol.* **2003**, *78*, 788.
[27] S. Bae, S. Gim, H. Kim, K. Hanna, *Appl. Catal. Environ.* **2016**, *182*, 541.
[28] S. Liu, J. Wang, W. Huang, X. Tan, H. Dong, B. A. Goodman, H. Du, F. Lei, K. Diao, *Chemosphere* **2019**, *214*, 821.

10990739, 2023, 3, Downloaded from https://onlinelibrary.wiley.com/doi/10.1002/aoc.7017 by T C Inonu University, Wiley Online Library on [19/02/2023]. See the Terms and Conditions (https://onlinelibrary.wiley.com/terms-and-conditions) on Wiley Online Library for rules of use; OA articles are governed by the applicable Creative Commons License

[29] D. Yu, L. Li, M. Wu, J. C. Crittenden, *Appl. Catal. Environ.* **2019**, *251*, 66.
[30] W.-Y. Ahn, S. A. Sheeley, T. Rajh, D. M. Cropek, *Appl. Catal. Environ.* **2007**, *74*, 103.
[31] M. Martin-Martinez, M. F. F. Barreiro, A. M. T. Silva, J. L. Figueiredo, J. L. Faria, H. T. Gomes, *Appl. Catal. Environ.* **2017**, *219*, 372.
[32] J. Li, C. Liu, Y. Liu, *J. Mater. Chem.* **2012**, *22*, 8426.
[33] L. Yu, J. F. Yang, B. Y. Guan, Y. Lu, X. W. D. Lou, *Angew. Chem. Int. Ed.* **2018**, *57*, 172.
[34] W.-J. Liu, K. Tian, H. Jiang, H.-Q. Yu, *Green Chem.* **2014**, *16*, 4198.
[35] X. Li, C. Zeng, J. Jiang, L. Ai, *J. Mater. Chem. A* **2016**, *4*, 7476.
[36] C. Chu, S. Rao, Z. Ma, H. Han, *Appl. Catal. Environ.* **2019**, *256*, 117792.
[37] M. He, J. Yao, Q. Liu, Z. Zhong, H. Wang, *Dalton Trans.* **2013**, *42*, 16608.
[38] C. C. Wagner, E. J. Baran, *Farm. Bonaerense* **2002**, *21*, 287.
[39] F. Hillman, J. M. Zimmerman, S. M. Paek, M. R. Hamid, W. T. Lim, H. K. Jeong, *J. Mater. Chem. A* **2017**, *5*, 6090.
[40] Y. Qian, Z. Liu, H. Zhang, P. Wu, C. Cai, *ACS Appl. Mater. Interfaces* **2016**, *8*, 32875.
[41] M. Kuang, Q. Wang, P. Han, G. Zheng, *Adv. Energy Mater.* **2017**, *7*, 1700193.
[42] S. Zhang, X. Xiao, T. Lv, X. Lv, B. Liu, W. Wei, J. Liu, *Appl. Surf. Sci.* **2018**, *446*, 10.
[43] M. K. Barman, A. K. Sinha, S. Nembenna, *Green Chem.* **2016**, *18*, 2534.
[44] B. B. Lu, J. Yang, G. B. Che, W. Y. Pei, J. F. Ma, *ACS Appl. Mater. Interfaces* **2018**, *10*, 2628.
[45] R. Murugan, M. B. Reddy, P. Pandurangan, R. Anandhan, *ACS Appl. Mater. Interfaces* **2020**, *12*, 56004.
[46] A. Schejn, A. Aboulaich, L. Balan, V. Falk, J. Lalevée, G. Medjahdi, R. Schneider, *Cat. Sci. Technol.* **2015**, *5*, 1829.
[47] Z. Xu, L. L. Han, G. L. Zhuang, J. Bai, D. Sun, *Inorg. Chem.* **2015**, *54*, 4737.
[48] Y. H. Hu, J. C. Wang, S. Yang, Y. A. Li, Y. B. Dong, *Inorg. Chem.* **2017**, *56*, 8341.
[49] P. Li, S. Regati, H. Huang, H. D. Arman, J. C. G. Zhao, B. Chen, *Inorg. Chem. Front.* **2015**, *2*, 42.
[50] I. Luz, F. L. Xamena, A. Corma, *J. Catal.* **2010**, *276*, 134.
[51] K. Naskar, S. Maity, H. S. Maity, C. Sinha, *Molecules* **2021**, *26*, 5296.
[52] X. Jia, G. Xu, Z. Du, Y. Fu, *Polyhedron* **2018**, *151*, 515.
[53] J. C. M. Willig, G. Granetto, D. Reginato, F. R. Dutra, É. F. Poruczinski, I. M. de Oliveira, G. V. Botteselle, *RSC Adv.* **2020**, *10*, 3407.
[54] Y. Wu, M. Xie, J. K. Jin, Z. Y. Zhang, H. Hu, Y. P. Tian, X. Jiang, *Small Struct.* **2022**, *3*, 2100155.
[55] H. Zhao, L. Zhao, *Dalton Trans.* **2018**, *47*, 3321.
[56] F. Ke, J. F. Zhu, L. G. Qiu, X. Jiang, *Chem. Commun.* **2013**, *49*, 1267.
[57] X. Q. Wu, D. D. Huang, Z. H. Zhou, W. W. Dong, Y. P. Wu, J. Zhao, D. S. Li, Q. C. Zhang, X. H. Bu, *Dalton Trans.* **2017**, *46*, 2430.
[58] A. Yazdi, F. Mercoçi, N. G. Bastús, I. Imaz, V. Puntes, D. Maspoch, *Cat. Sci. Technol.* **2016**, *6*, 8388.
[59] X. K. Song, H. Z. Sun, X. Cao, Z. X. Wang, D. J. Zhao, J. H. Sun, H. J. Zhang, X. P. Li, *RSC Adv.* **2016**, *6*, 112451.
[60] Y. Wang, Q. Li, P. Zhang, D. O'Connor, R. S. Varma, M. Yu, D. Hou, *J. Colloid Interface Sci.* **2019**, *539*, 161.
[61] W. Zhang, F. Tan, W. Wang, X. Qiu, X. Qiao, J. Chen, *J. Hazard. Mater.* **2012**, *217*, 36.
[62] B. Zheng, X. Liu, Y. Wu, L. Yan, J. Du, J. Dai, Q. Xiong, Y. Guo, D. Xiao, *Inorg. Chem. Front.* **2017**, *4*, 1268.
[63] T. A. Revathy, S. Dhanavel, T. Sivaranjani, V. Narayanan, T. Maiyalagan, A. Stephen, *Appl. Surf. Sci.* **2018**, *449*, 764.
[64] G. Wu, X. Liang, L. Zhang, Z. Tang, M. Al-Mamun, H. Zhao, X. Su, *ACS Appl. Mater. Interfaces* **2017**, *9*, 18207.
[65] F. Wang, S. Song, K. Li, J. Li, J. Pan, S. Yao, X. Ge, J. Feng, X. Wang, H. Zhang, *Adv. Mater.* **2016**, *28*, 10679.
[66] X. Zhang, L. Geng, Y.-Z. Zhang, D.-S. Zhang, R. Zhang, J. Fu, J. Gao, J. C. Carozza, Z. Zhou, H. Han, *CrstEngComm* **2019**, *21*, 5382.
[67] X. Zhang, N. Wang, L. Geng, J. Fu, H. Hu, D. Zhang, B. Zhu, J. Carozza, H. Han, *J. Colloid Interface Sci.* **2018**, *512*, 844.
[68] B. Xu, X. Li, Z. Chen, T. Zhang, C. Li, *Micropor. Mesopor. Mater.* **2018**, *255*, 1.
[69] H. Jiang, Q. Yan, R. Chen, W. Xing, *Micropor. Mesopor. Mater.* **2016**, *225*, 33.
[70] H. Zhang, S. Qi, X. Niu, J. Hu, C. Ren, H. Chen, X. Chen, *Cat. Sci. Technol.* **2014**, *4*, 3013.
[71] D. Zhang, L. Chen, G. Ge, *Catal. Commun.* **2015**, *66*, 95.

SUPPORTING INFORMATION

Additional supporting information can be found online in the Supporting Information section at the end of this article.

How to cite this article: N. Buğday, S. Yaşar, S. Altin, O. Duygulu, Y. Önal, *Appl Organomet Chem* **2023**, *37*(3), e7017. https://doi.org/10.1002/aoc.7017

10990739, 2023, 3, Downloaded from https://onlinelibrary.wiley.com/doi/10.1002/aoc.7017 by T C Inonu University, Wiley Online Library on [19/02/2023]. See the Terms and Conditions (https://onlinelibrary.wiley.com/terms-and-conditions) on Wiley Online Library for rules of use; OA articles are governed by the applicable Creative Commons License